Biophysical Journal
Article

Biophysical Society

pH-Dependent Interactions in Dimers Govern the Mechanics and Structure of von Willebrand Factor

Jochen P. Müller,[1,*] Achim Löf,[1] Salomé Mielke,[1] Tobias Obser,[2] Linda K. Bruetzel,[1] Willem Vanderlinden,[1,3] Jan Lipfert,[1] Reinhard Schneppenheim,[2] and Martin Benoit[1]

[1]Department of Physics and Center for Nanoscience, LMU Munich, Munich, Germany; [2]Department of Pediatric Hematology and Oncology, University Medical Center Hamburg-Eppendorf, Hamburg, Germany; and [3]Department of Chemistry, Division of Molecular Imaging and Photonics, KU Leuven–University of Leuven, Leuven, Belgium

ABSTRACT Von Willebrand factor (VWF) is a multimeric plasma glycoprotein that is activated for hemostasis by increased hydrodynamic forces at sites of vascular injury. Here, we present data from atomic force microscopy-based single-molecule force measurements, atomic force microscopy imaging, and small-angle x-ray scattering to show that the structure and mechanics of VWF are governed by multiple pH-dependent interactions with opposite trends within dimeric subunits. In particular, the recently discovered strong intermonomer interaction, which induces a firmly closed conformation of dimers and crucially involves the D4 domain, was observed with highest frequency at pH 7.4, but was essentially absent at pH values below 6.8. However, below pH 6.8, the ratio of compact dimers increased with decreasing pH, in line with a previous transmission electron microscopy study. These findings indicated that the compactness of dimers at pH values below 6.8 is promoted by other interactions that possess low mechanical resistance compared with the strong intermonomer interaction. By investigating deletion constructs, we found that compactness under acidic conditions is primarily mediated by the D4 domain, i.e., remarkably by the same domain that also mediates the strong intermonomer interaction. As our data suggest that VWF has the highest mechanical resistance at physiological pH, local deviations from physiological pH (e.g., at sites of vascular injury) may represent a means to enhance VWF's hemostatic activity where needed.

INTRODUCTION

To prevent excessive blood loss at sites of vascular injury, damaged vessel walls need to be sealed rapidly and effectively by a hemostatic plug. A key player in the formation of a hemostatic plug is the multimeric plasma glycoprotein von Willebrand factor (VWF). Activated by increased hydrodynamic forces at sites of vascular injury, VWF critically mediates hemostasis by binding to subendothelial collagen and promoting platelet aggregation (1–3). VWF's central role in hemostasis is underlined by a variety of mutations in VWF that cause the common bleeding disorder von Willebrand disease (4).

The complex biosynthesis of linear VWF multimers (concatamers) in vascular endothelial cells and megakaryocytes involves extensive posttranslational processing (4,5), some steps of which crucially depend on pH-regulated conformational changes of the protein (6,7). After expression as preproproteins—comprising a short signal peptide sequence and propeptide domains D1 and D2 in addition to the domains present in mature VWF (D′D3, A1, A2, A3, D4, C1-C6, and CK; see Fig. 1 *A*)—and subsequent cleavage of the signal peptide, monomers are dimerized in the endoplasmic reticulum (ER, pH 7.4) in a tail-to-tail fashion via disulfide linkage between their C-terminal CK domains (5,8). Dimers are equipped with N- and O-linked glycans in the ER and the Golgi, respectively (5). At the lowered pH values of the Golgi and *trans*-Golgi (pH 6.2), dimers were shown to preferentially adopt a compact conformation, as monomers zip up from the CK domains to the A2 domains to form so-called dimeric bouquets (7). However, A2 and A3 are not crucial for bouquet formation (7). Such compact dimeric bouquets are thought to favor the formation of closely packed helical tubules built up from dimers in the *trans*-Golgi and Weibel-Palade bodies (6,9). The latter are secretory granules of endothelial cells and have a pH of ~5.4 (10), close to VWF's isoelectric point (pI) (11). Tubule formation crucially depends on pH-regulated association of the propeptide domains D1 and D2 (5,6), and goes hand in hand with orderly linear multimerization

Submitted April 11, 2016, and accepted for publication June 21, 2016.

*Correspondence: jochen.mueller@physik.uni-muenchen.de

Jochen P. Müller and Achim Löf contributed equally to this work.

Editor: Daniel Muller.

http://dx.doi.org/10.1016/j.bpj.2016.06.022

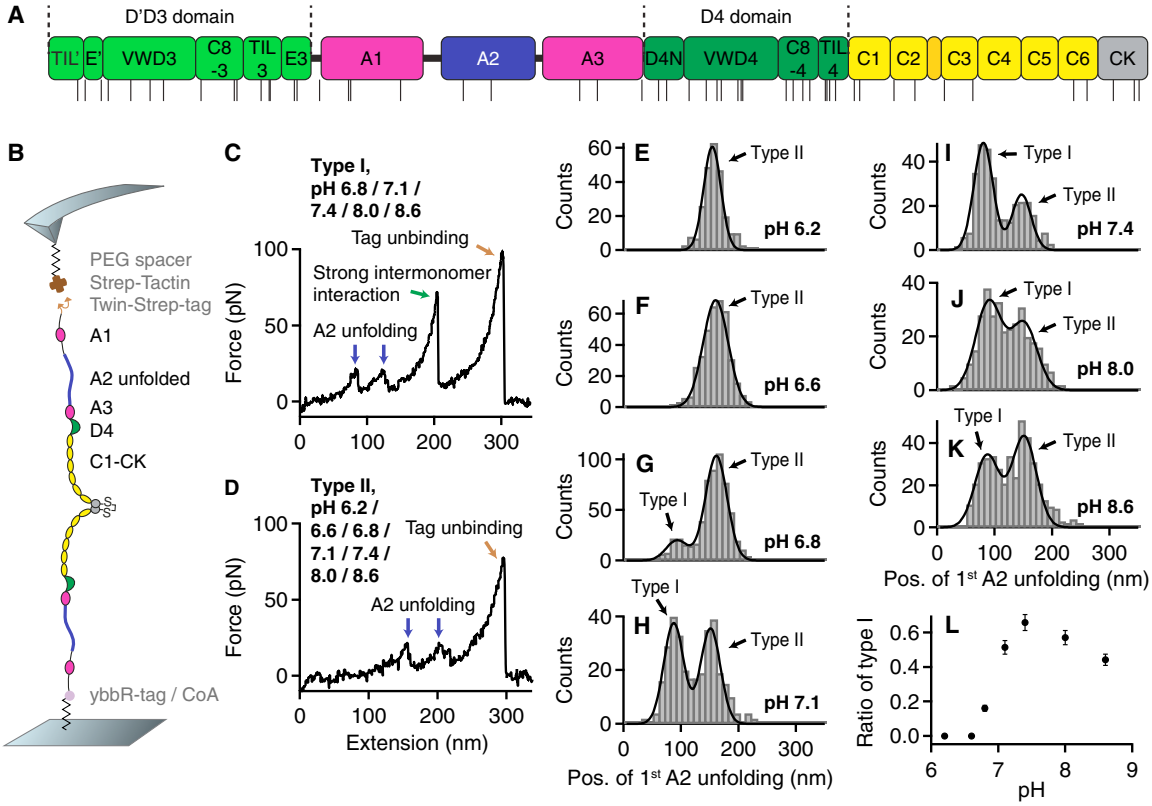

FIGURE 1 Single-molecule force measurements on dimeric VWF A1-CK constructs under varied pH conditions. (*A*) Domain organization of mature VWF (residues 764–2813) as described in (1,12). The positions of histidine residues are indicated by the black lines beneath. (*B*) Schematic of pulling dimeric A1-CK constructs (not drawn to scale). (*C* and *D*) Denoised force-extension traces of type I and type II characterized by A2 unfolding peaks (*blue arrows*) at low (type I) and high (type II) extension values, respectively. Type II traces were observed throughout the probed pH range, whereas type I traces, showing the force response of dimers that were initially firmly closed via the strong intermonomer interaction (13), were essentially obtained only at pH values of $\geq$6.8. For all pH values at which type I traces were observed, dissociation of the strong intermonomer interaction (*green arrow*) yielded unvaried characteristic length increments. The final peak (*brown arrow*) corresponds to tag unbinding, i.e., to dissociation of the specific Twin-Strep-tag/Strep-Tactin interaction and rupture of the probed molecule from the AFM tip (13,34). (*E* and *F*) Unimodal distributions of the position of the first A2 unfolding peak obtained at pH 6.2 (*E*, $n = 253$) and 6.6 (*F*, $n = 385$). The distributions are well described by fits of Gaussian functions (*solid lines*). (*G–K*) Bimodal distributions of the position of the first A2 unfolding peak obtained at pH values of 6.8 (*G*, $n = 586$), 7.1 (*H*, $n = 329$), 7.4 (*I*, $n = 317$), 8.0 (*J*, $n = 336$), and 8.6 (*K*, $n = 428$). To estimate the ratio of type I and type II traces, the distributions were fitted with double Gaussian functions (*solid lines*). (*L*) Ratio of type I traces as a function of the pH. Error bars represent Poisson noise (1 SD). To see this figure in color, go online.

of dimers (6,7). Templated by the tubule architecture, linkage of dimers occurs in a head-to-head fashion via the formation of disulfide bonds between N-terminal D′D3 domains (5,7), resulting in concatamers built up from dimers as the smallest repeating subunits, which after proteolytic cleavage of the propeptide possess a mass of ~500 kDa. It was speculated that histidine residues in VWF's C-terminal segment D4-CK mediate pH-dependent bouquet formation (7). Indeed, several of VWF's domains harbor a comparably large number of histidines (Fig. 1 *A*). The highest density of histidines is found in VWF's D4 domain, which is an assembly of distinct submodules (D4N, D4, C8-4, and TIL4) (12).

Upon secretion into the vasculature, VWF encounters a pH of 7.4 and adopts an overall more flexible conformation (1). However, we recently showed that a strong intermonomer interaction is present in roughly half of VWF's dimeric subunits under near-physiological conditions (13). In brief, atomic force microscopy (AFM)-based single-molecule force measurements on VWF dimers revealed two types of characteristic force-extension traces. While type II traces only exhibited peaks corresponding to the well-characterized unfolding of the A2 domains (~10–20 pN) (14–17), type I traces revealed an additional peak at high force (>50 pN) that was identified with the dissociation of a strong intermonomer interaction, which provided an additional length of ~80 nm to the elongation of dimers. Our data further revealed that this interaction critically involves the D4 domain and divalent ions. In the bloodstream, elongational forces on VWF result from the interplay of an elongational flow component and VWF's extraordinary length (14,18), which may exceed 15 μm in the plasma (2). Force sensing, i.e., the conversion of flow into a physiological signal, is crucial for VWF's hemostatic function, as

VWF's activation for collagen binding and binding to the platelet glycoprotein Ib (GPIb) was shown to be force-induced (2,3). Increased forces acting on VWF are encountered where elongational flow components are elevated, as for instance at sites of vascular injury, but also in stenosed vessels, where VWF can provoke thrombosis (1). Importantly, by reducing the effective force-sensing length of concatamers, the strong intermonomer interaction in VWF's dimeric subunits can be assumed to increase critical rates of elongational flow to activate VWF for hemostasis (13).

While the pH crucially affects VWF's conformation, it has not been clarified to what extent it influences VWF's mechanics, i.e., its response to external forces. It has been proposed that pH variations may play a pivotal role in VWF's activation by affecting critical rates of elongational flow (19). Certainly, the pH in healthy blood vessels is precisely buffered to maintain a pH of 7.4, and small deviations of 0.1 already represent pathophysiological conditions. However, as suggested by several studies (20–24), the pH may vary locally at sites of injury and inflammation. Furthermore, to shed light on the nature of the molecular mechanisms underlying VWF's structure and mechanics, in particular regarding the strong intermonomer interaction, a comprehensive investigation of the influence of the pH is of general interest.

Here, we present data from AFM-based single-molecule force measurements, AFM imaging, and small-angle x-ray scattering (SAXS). Our results show that the ratio of dimers that exhibit the strong intermonomer interaction strongly depends on the pH and reaches a maximum at pH 7.4. Dimers were in the focus of our investigations because they build up higher-order concatamers without significantly changing their individual structure (13). Our data further reveal that compactness of dimers under acidic conditions is accomplished by another intermonomer interaction that has, however, a lower mechanical resistance. Overall, we combine force and imaging data to dissect and locate pH-dependent interactions within VWF's dimeric subunits and to characterize their mechanical resistance, which crucially affects force sensing by VWF and thus VWF's activation for hemostasis.

MATERIALS AND METHODS

Genetic engineering of recombinant proteins

Heterodimeric VWF constructs were expressed in HEK 293 cells (DSMZ, Braunschweig, Germany) after the cells were initially cotransfected with two different plasmids encoding the VWF sequence and N-terminal ybbR- or N-terminal Twin-Strep-tag, respectively (13). The constructs used for AFM imaging experiments possessed a Strep-tag instead of the Twin-Strep-tag. VWF monomers were expressed in HEK 293 cells after the cells were transfected with a single type of plasmid encoding the VWF sequence and both N-terminal ybbR-tag and C-terminal Twin-Strep-tag. Plasmid construction was carried out as previously described in detail (13). Cells were transfected in Dulbecco's modified Eagle's medium (Life Technologies, Darmstadt, Germany) containing 10% fetal bovine serum (Life Technologies), 4 μg plasmid (for cotransfection 2 μg of both plasmids), and 15 μL Lipofectamine 2000 (Life Technologies). At 24 h after transfection, the cells were transferred into a selection medium containing 500 μg/mL G418 (Invivogen, Toulouse, France). In the case of cotransfected cells, the selection medium additionally contained 250 μg/mL Hygromycin B (Invivogen). After 2–3 weeks, the polyclonal cell culture was seeded for expression. After 72 h of cell growth, the medium was exchanged against OPTIPRO-SFM (Life Technologies) for secretion of recombinant VWF. The culture supernatant was collected after 72 h and subsequently concentrated using Amicon Ultra-15 MWCO 100 kDa (Merck Chemicals, Schwalbach, Germany).

Strep-Tactin with a single cysteine, which was used to specifically pull Twin-Strep-tagged VWF, was prepared as described in (13,25).

Buffers

For experiments under varied pH conditions, we used buffer solutions containing 150 mM NaCl and 20 mM of one of the following buffering agents: Na-acetate (pH 5.4), BisTris (pH 6.2, 6.6, and 6.8), Hepes (pH 7.1 and 7.4), or Tris (pH 8.0 and 8.6). The pH was adjusted using HCl and NaOH, respectively. Buffers used for measurements in the presence of divalent ions additionally contained 1 mM $CaCl_2$ and 1 mM $MgCl_2$. Buffers used for measurements in the presence of free Imidazole further contained 200 mM Imidazole in addition to $CaCl_2$ and $MgCl_2$. Prior to measurements in the absence of divalent ions, proteins were incubated with 10 mM EDTA for 8 h and the buffer was exchanged to the measurement buffer. For SAXS measurements in the absence of divalent ions, the buffers still contained 10 mM EDTA. Since SAXS requires much larger amounts of protein than the single-molecule techniques, we refrained from an additional buffer exchange to buffer without EDTA to minimize sample loss. The presence of EDTA in the measurement buffer, compared with the initial incubation with buffer containing EDTA and subsequent buffer exchange, did not affect the ratios of compact dimers observed in AFM imaging, as verified for pH 6.2 and 7.4 (Fig. S5 in the Supporting Material).

Single-molecule force measurements

For single-molecule force measurements, samples and cantilevers were prepared as previously described (13). In brief, VWF constructs carrying a ybbR-tag (DSLEFIASKLA) and a Twin-Strep-tag (WSHPQFEKG GGSGGGSGGGSWSHPQFEK) were covalently attached to a glass surface functionalized with coenzyme A (CoA). For preparation of CoA-functionalized surfaces, glass slides were initially silanized with (3-aminopropyl)-dimethyl-ethoxysilane (APDMES) (26). Afterward, a 5 kDa N-hydroxy-succinimide-polyethylene glycol-maleimide linker (PEG linker, 25 mM) was conjugated to amine groups on the glass surface. The maleimide group of the PEG linker allowed for subsequent coupling of CoA (25 mM) to the PEGylated glass surfaces. Effective coupling was achieved at pH 7.2 in buffer containing 50 mM sodium phosphate, 50 mM NaCl, and 10 mM EDTA. Finally, the CoA-functionalized slides were incubated with VWF constructs (1 mg/mL) in OPTIPRO-SFM medium, in the presence of Sfp-transferase and $MgCl_2$. The slides were incubated overnight at pH 7.4 and 4°C. After incubation, the slides were carefully rinsed with buffer, ensuring a permanent liquid environment for immobilized proteins and a loss of nonimmobilized proteins.

In a manner similar to that used for surfaces, AFM cantilevers with a silicon tip (BL-AC40TS-C2; Olympus, Tokyo, Japan) were silanized with APDMES and incubated with the 5 kDa PEG linker (25 mM). Afterward, Strep-Tactin bearing a single cysteine residue (Strep-Tactin-Cys) was covalently attached to maleimide groups at the cantilever surface (13,25). Before incubation, Strep-Tactin-Cys was reduced in the presence of tris(2-carboxyethyl)phosphine beads and then separated from them by filtering. The cantilevers were then incubated with the reduced Strep-Tactin-Cys (10 mM) for 3 h. Before experiments were conducted, the cantilevers were relocated into the respective buffer for each experiment.

Single-molecule force measurements were carried out as described previously (13) using custom-built instruments (27), each controlled by an MFP-3D controller (Asylum Research, Santa Barbara, CA). The cantilever spring constants were determined using the thermal noise method (28). The cantilever was brought into contact with the sample surface and retracted at six different pulling speeds ranging from 0.2 to 6.4 μm/s. The sample was displaced in the *x-y* direction after each force-extension trace to probe different molecules.

Force-extension traces were subjected to total variation denoising (TVD) and then further analyzed (29). To separate specific pulling events from unspecific ones, we used A2 unfolding peaks as a positive fingerprint (13). At pH values of $\leq$7.4, ~2% of the total number of traces, which also includes traces that did not reveal any adhesion between the cantilever tip and a molecule, exhibited the fingerprint of two A2 unfolding peaks in A1-CK dimers. At the alkaline pH values of 8.0 and 8.6, however, the yield of traces that showed clear A2 unfolding peaks was significantly decreased to ~0.5%. To estimate the ratio of type I and type II traces for pH values of $\geq$6.8, the bimodal distributions of the position of the first A2 unfolding peak were fitted with a double Gaussian function. More precisely, five free parameters were fitted: the peak amplitudes and positions for both peaks individually and a single value for the width of either peak, accounting for experimental uncertainties that are virtually the same for type I and type II traces. To generate characteristic overlays of force-extension traces, undenoised force-extension traces were used. Traces were offset (offsets within 20 nm) along the extension axis to achieve alignment with respect to the stretch before the rupture peak.

AFM imaging

Heterobifunctional dimeric VWF constructs (either full-length dimers or dimers with a deletion of the D4 domain), carrying both N-terminal Strep-tags and ybbR-tags, were purified using a HiTrap StrepTrap column (GE Healthcare Europe, Freiburg, Germany). Eluates were buffer exchanged to the respective measurement buffer and concentrated by centrifuge filtration using Amicon Ultra-15 MWCO 100 kDa.

Substrates were prepared as previously described (13). In brief, freshly cleaved mica sheets (grade I; SPI Supplies, West Chester, PA) were incubated with 20 μL of a poly-L-lysine (PLL) solution (molecular weight 500–2000; 0.01% w/v (Sigma-Aldrich); in ultrapure water) for 30 s. Afterward, they were thoroughly rinsed with 25 mL of ultrapure water and dried in a stream of nitrogen. Then, 20 μL of buffer solution containing ~5 μg/mL of VWF constructs was deposited on the functionalized mica substrates and incubated for 30 s. Finally, the substrates were rinsed with 20 mL of ultrapure water and dried in a stream of nitrogen.

AFM images of 1 μm $\times$ 1 μm and 1024 $\times$ 1024 pixels were recorded in tapping mode in air using an MFP-3D atomic force microscope (Asylum Research) and cantilevers with silicon tips (AC160TS; Olympus). These cantilevers have a nominal spring constant of 26 N/m and a resonance frequency of ~300 kHz. Raw image data were processed and analyzed using SPIP software (v6.4.4; Image Metrology, Hørsholm, Denmark). Image processing involved plane correction (third-order polynomial plane-fitting and flattening according to the histogram alignment routine) and Gaussian filtering.

Dimer conformations were analyzed by tracing dimers individually along their contour, following local maxima in height, employing polyline profiling. To quantify the compactness of a dimer, we measured its stem length, i.e., the distance along the contour between the CK domain and the position at which the two constituent monomers separate from each other. We additionally determined the distance from the CK domain to the beginning of higher N-terminal domains for the two constituent monomers and used the mean of these distances to normalize the stem length.

For the sigmoidal fit shown in Fig. 3 *C*, the following function was used:

$$y = y_{\max} / \{1 + \exp[(x_{\text{half}} - x)/rate]\}$$

SAXS data acquisition and analysis

For SAXS measurements, samples of A1-CK dimers carrying an N-terminal Twin-Strep-tag were prepared as described previously (13). Measurements were performed at beamline P12 (Deutsches Elektronen Synchrotron, Hamburg, Germany) (see Fig. 3 *D*) (30), as described in (13), and at beamline X12SA (cSAXS) at the Swiss Light Source (Paul Scherrer Institute, Villigen, Switzerland) (Fig. S6). Measurements at beamline X12SA employed an x-ray energy of 12.4 keV and a sample-to-detector distance of 7 m, resulting in a q range of ~(0.04 – 1.5) nm^{-1} (with $q = 4\pi \sin(\theta)/\lambda$, where 2θ is the total scattering angle and λ is the x-ray wavelength). Sample solutions were added to 1-mm-diameter quartz capillaries and kept at room temperature. Data were acquired with an exposure time of 1 s each at 10 positions along the length of the capillary. For all samples, the 10 profiles showed no signs of radiation damage. Matching profiles were averaged. Corresponding buffer samples were measured using identical procedures, and buffer profiles were subtracted for background correction. To display the data in Kratky representation (intensity $I(q) \times q^2$ vs. q), we scaled the data by a constant factor. To compute the pair distance distribution functions $P(r)$, we used the program PRIMUS (31).

RESULTS

Force response of dimeric VWF under varied pH conditions

For single-molecule force measurements, we used heterobifunctional VWF constructs (13) composed of two A1-CK monomers (aa 1238–2813) with different N-terminal tags (Fig. 1 *B*). Dimeric A1-CK constructs were preferred over full-length constructs because they resulted in significantly increased yields of specific pulling events. Higher yields may be a result of the tags being more accessible when located at the native linker N-terminal of A1 than when located directly at the N-terminus of D′D3. A ybbR-tag at the N-terminus of one of the A1-CK monomers enabled covalent attachment to a CoA-functionalized glass surface (32), and a Twin-Strep-tag at the N-terminus of the other A1-CK monomer allowed for specific pulling via a Strep-Tactin-functionalized AFM cantilever (33). We used PEG spacers at both the glass surface and the cantilever to minimize unspecific protein–surface interactions.

We performed single-molecule force measurements under different pH conditions, ranging from pH 6.2 to pH 8.6, while keeping the ionic conditions fixed (150 mM NaCl, 1 mM $CaCl_2$, 1 mM $MgCl_2$). We adjusted the different pH values by buffer exchange, after attachment of the constructs to the functionalized surface at a pH of 7.4. Force-extension traces corresponding to specific pulling events were identified by using the appearance of two A2 unfolding peaks as a positive fingerprint (13). For all probed pH values, traces corresponding to specific pulling events did not exhibit any further characteristic peaks except those of A2 unfolding and, in type I traces, the high-force peak corresponding to the dissociation of the strong intermonomer interaction in initially firmly closed dimers. Type I and type II traces exhibited A2 unfolding peaks at low

and high extension values, respectively (first A2 unfolding peak at roughly 80 and 150 nm, respectively) (13).

While type I traces were only observed at pH values of ≥6.8 (Fig. 1 *C*), type II traces were observed at all examined pH values (Fig. 1 *D*). In other words, at a pH of 6.2 and 6.6, only type II traces were observed (Fig. S1), whereas at pH values of ≥6.8, both type I and type II traces were obtained (Fig. S2), albeit with markedly varied ratios. Accordingly, quantifying the position of the first A2 unfolding peak in force-extension traces yielded unimodal distributions for pH 6.2 and 6.6 (Fig. 1, *E* and *F*), and characteristic bimodal distributions for pH values of ≥6.8 (Fig. 1, *G–K*). These distributions revealed that for both type I and type II traces, the mean values of the positions of first A2 unfolding were conserved throughout the probed pH range within a standard deviation (SD) of 5 nm, showing that no domains were significantly destabilized by acidic pH, e.g., due to destabilized disulfide bonds. In line with this, force-extension traces of VWF monomers (D′D3-CK) at pH 6.2 were essentially identical to those obtained at pH 7.4 (Fig. S3). We estimated the ratios of type I and type II traces for pH ≥ 6.8 from double Gaussian fits to the distributions of the first A2 unfolding position. The ratio of type I traces as a function of the pH exhibited an abrupt increase at pH ~7.0 and a maximum value of (66 ± 5)% at pH 7.4 (Fig. 1 *L*), closely matching the ratio previously observed for full-length dimers (13). Upon further alkalization, the ratio of type I traces slightly decreased, resulting in a value of (44 ± 3)% at pH 8.6. It should be noted that at both pH 8.0 and 8.6, the yield of specific pulling events (i.e., force-extension traces exhibiting two clear A2 unfolding peaks) was lower than at pH ≤ 7.4. Overall, these data show that the formation of the strong intermonomer interaction in VWF's dimeric subunits strongly depends on the pH.

To test for reversibility of the underlying molecular mechanisms, we exchanged the buffer of immobilized proteins after measurements at pH 6.6 (histogram of the first A2 unfolding position shown in Figs. 1 *F* and 2 *A*) to buffer solution adjusted to pH 7.4. Importantly, force-extension traces of type I were recovered, indicating that the pH-dependent mechanisms that critically affect the formation of firmly closed dimers are largely reversible. However, the ratio of type I traces was lower [(35 ± 3)%] than it was in experiments without prior incubation at acidic pH, as inferred from the bimodal distribution of the position of the first A2 unfolding (Fig. 2 *B*).

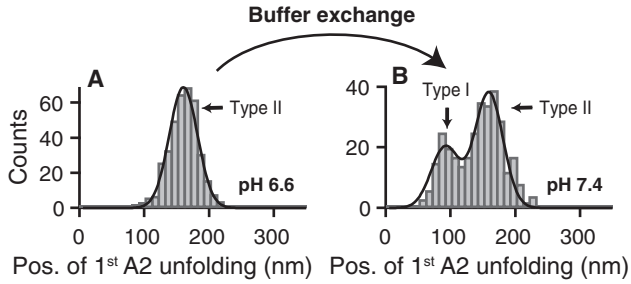

FIGURE 2 Reversibility of the pH-dependent mechanisms affecting the formation of the strong intermonomer interaction in VWF's dimeric subunits. (*A*) Unimodal distribution of the position of the first A2 unfolding peak in force-extension traces of A1-CK dimers measured at pH 6.6 (same histogram as shown in Fig. 1 *F*, $n = 385$), indicating that only type II traces were observed. (*B*) Histogram of the position of the first A2 unfolding peak, obtained after buffer exchanging immobilized proteins to a buffer solution with pH 7.4 ($n = 323$) and with the same cantilever that was used at pH 6.6. The bimodality of the distribution indicates that a significant number of type I traces were observed, proving that the molecular mechanisms that critically affect the pH-dependent formation of the strong intermonomer interaction are largely reversible. Fitting a double Gaussian (*solid line*) yielded a ratio of (35 ± 3)% type I traces. To see this figure in color, go online.

Conformational ensemble of VWF dimers under varied pH conditions

To complement the single-molecule force experiments, we employed AFM imaging to assess the conformations of dimeric VWF constructs adsorbed onto a PLL-coated mica substrate under different pH conditions (see "Buffers" section in Materials and Methods, and example images in Fig. 3, *A* and *B*). We quantified the ratio of compact dimers by analyzing the conformation of each dimer individually. In detail, we determined the stem length for each dimer, i.e., the distance along the contour from the CK domain to the position at which the two constituent monomers separate from each other. We further measured the distance along the contour between the CK domain and the beginning of higher N-terminal domains for both monomers, and used the mean of these distances to normalize the stem length. In general, the distributions of this normalized stem length exhibited two distinct populations corresponding to dimers with (partially) open stems and fully formed ones, respectively (Fig. S4). Dimers corresponding to the second population, exhibiting a normalized stem length above 1, were assigned as compact (13). It should be noted that at alkaline pH values, a nonnegligible fraction of molecules—up to ~40% at pH 8.6— had to be discarded from analysis because apparent self-aggregation repeatedly impeded unequivocal tracing, in line with observations from an earlier transmission electron microscopy study (7).

We determined the ratio of compact full-length dimers (D′D3-CK) as a function of pH in both the presence (Fig. 3 *C*, *blue circles*) and additionally in the absence (Fig. 3 *C*, *red triangles*) of divalent ions, i.e., under conditions that obstruct the formation of the strong intermonomer interaction (13). In the latter case, to remove divalent ions from solution, samples were incubated with EDTA before buffer exchange to the measurement buffer. In the absence of divalent ions, compactness decreased monotonically with increasing pH and was very well described by the fit of a simple sigmoidal function (Fig. 3 *C*, *dashed line*), reaching its half-maximum at a pH of ~6.6. These findings

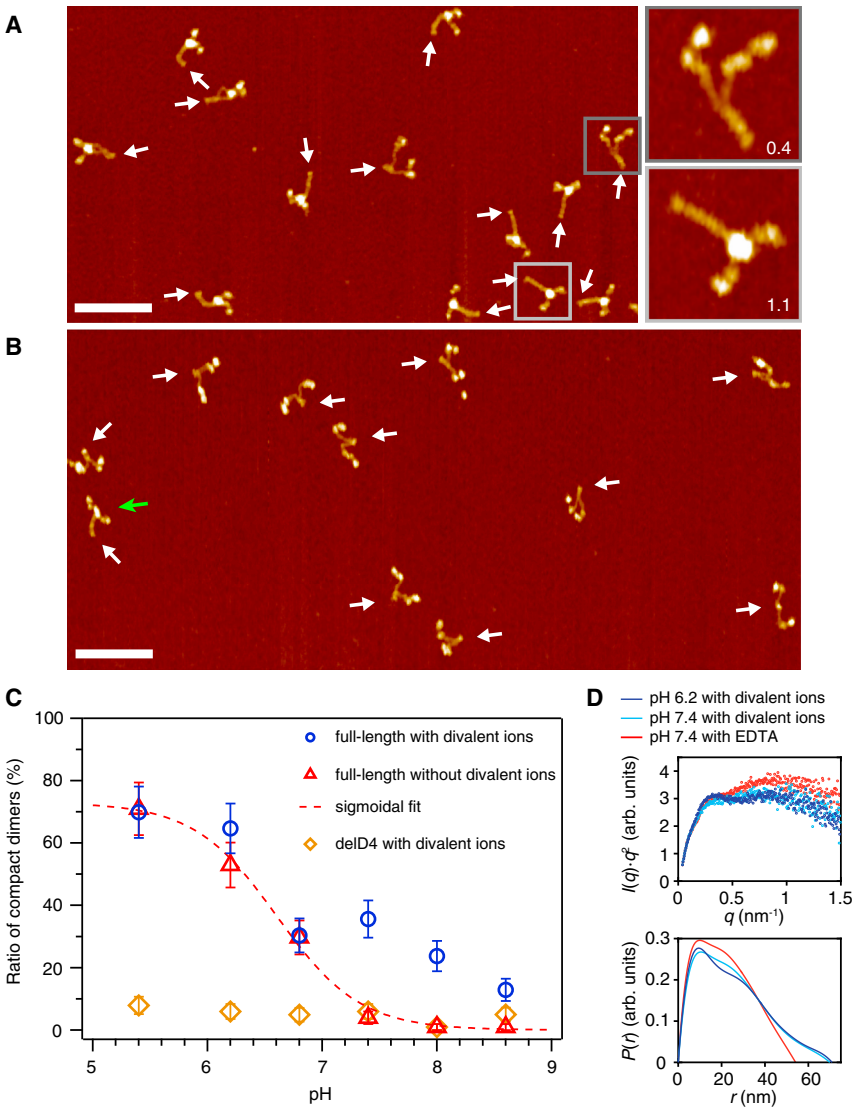

FIGURE 3 Conformation of dimeric VWF constructs under varied pH and ionic conditions. (*A*) Representative AFM image of full-length VWF dimers (D′D3-CK) adsorbed onto a functionalized mica surface from buffer solution without divalent ions and adjusted to pH 6.2. Arrows mark the positions of CK domains. A large fraction (>50%) of dimers exhibited a compact conformation with fully formed C-terminal stems. Insets show examples of a flexible dimer with a partially formed stem and a compact dimer with a fully formed stem, respectively. Numbers indicate values of the normalized stem length. Scale bar is 100 nm; range of color scale is 2.4 nm. (*B*) Representative AFM image of VWF dimers with a deletion of the D4 domain (delD4 dimers), adsorbed onto a functionalized mica substrate from buffer solution adjusted to pH 6.8 and containing divalent ions. White arrows mark the positions of CK domains. Throughout the whole probed pH range, nearly all delD4 dimers exhibited a flexible conformation. The green arrow indicates an occasional compact dimer. Scale bar is 100 nm; range of color scale is 2.4 nm. (*C*) Ratio of compact VWF dimers as a function of the pH. Only dimers with a normalized stem length above 1 were assigned as compact. Shown are data for full-length dimers in the presence (*blue circles*) and absence (*red triangles*) of divalent ions, and for delD4 dimers in the presence of divalent ions (*brown squares*). The dashed red line is a sigmoidal fit (half-maximum value at pH 6.6) to the data obtained for full-length dimers in the absence of divalent ions, i.e., under conditions that obstruct the formation of the strong intermonomer interaction mediated by the D4 domain (13). Error bars represent Poisson noise (1 SD). For each data point, $n \geq 100$ dimers were analyzed. (*D*) SAXS profiles in Kratky representation (*top*) and computed distance distribution functions $P(r)$ (*bottom*) for dimeric A1-CK constructs in the presence of divalent ions at pH 6.2 (*dark blue*) and pH 7.4 (*light blue*), and in the presence of 10 mM EDTA at pH 7.4 (*red*). To see this figure in color, go online.

suggest that compactness is mainly driven by a single process in the absence of divalent ions. In the presence of divalent ions, for pH values of $\leq$6.8, we obtained ratios of compact dimers essentially identical to those observed in the absence of divalent ions. Above a pH of 6.8, however, a second regime of compactness was observed. Intriguingly, the deviation from the data obtained in the absence of divalent ions was highest at a pH of 7.4. These findings are in line with the pH dependence of the strong intermonomer interaction observed in force measurements.

For further structural characterization, we performed SAXS measurements on A1-CK dimers at pH 6.2 and 7.4, both in the presence of divalent ions and in the presence of EDTA. SAXS is a solution-based technique that does not require immobilization of samples on to a surface, making it a complementary tool to dissect conformational changes of dimeric VWF upon varying solution conditions in bulk (35,36). We observed a conformational transition when the pH was changed from 6.2 (Fig. 3 *D*, *top*, *dark blue*) to 7.4 (*light blue*) in the presence of divalent ions, as revealed by the SAXS profiles in Kratky representation. For both solution conditions, the Kratky plots exhibit a plateau shape with two slight peaks. However, at the lower pH value, the peaks are more pronounced and the intensity is lower at higher q-values, implying more compact and less flexible dimers at pH 6.2 than at pH 7.4. SAXS data were further acquired in the presence of EDTA, i.e., under conditions that obstruct the formation of the strong intermonomer interaction. At pH 7.4, we observed a transition to an ensemble of more flexible conformations (13), indicated by a more diverging shape at high q-values and less pronounced peaks in the Kratky plot (Fig. 3 *D*, *top*, *red*). In contrast, at pH 6.2, no significant change was observed upon addition of EDTA (Fig. S6). These findings are further corroborated by a comparison of the pair distance distribution functions $P(r)$ (histograms of pairwise distances in the molecule, Fig. 3 *D*,

bottom). In the presence of divalent ions, the shape of the $P(r)$ function is indicative of a rather extended, rod-like molecule, even more pronounced at pH 6.2 than at pH 7.4. In contrast, upon addition of EDTA at pH 7.4, a shortening and steeper decay of $P(r)$ was observed, indicating a more flexible and thus more globular ensemble of dimer conformations. Overall, the SAXS data are fully in line with the results from AFM imaging.

Furthermore, again employing AFM imaging, we studied the compactness of dimers with a deletion of the D4 domain (aa 1873–2255; delD4 dimers) in the presence of divalent ions (Fig. 3 *C*, *brown squares*). Throughout the whole pH range, compact dimers were observed only occasionally (Fig. 3 *B*), strongly suggesting that the D4 domain plays a key role not only in forming the strong intermonomer interaction (13), but also in promoting the compactness of dimers under acidic pH conditions.

We further observed that the pH also affected the formation of C-terminal stems (7,13). To investigate this effect without the influence of D4-mediated interactions, we analyzed the distributions of the normalized stem length for the delD4 construct (Fig. 4), which exhibited virtually only values of the normalized stem length below 1, corresponding to flexible dimers. In general, higher average stem lengths were favored by low pH, even in the absence of D4-mediated interactions promoting compactness. In particular, also the functional shape of the stem length distributions changed considerably with the pH. While at alkaline pH values the distribution of the normalized stem length exhibited an approximately exponential shape, at lower pH values it revealed a maximum centered at roughly 0.4 that became more prominent with decreasing pH, suggesting that the different C-domain interactions involved in stem formation are differently affected by the pH. The maximum centered at ~0.4 corresponds to dimers possessing roughly half-formed C-terminal stems, i.e., stems that are formed from CK domains up to a region comprising domains C5–C3, which interestingly exhibit a comparably low density of histidine residues (Fig. 1 *A*).

Obstruction of the strong intermonomer interaction by Imidazole

The data presented above indicate that the strong intermonomer interaction is most favorable at pH 7.4 and only occurs in the presence of divalent ions. We aimed to gain further insight into the underlying molecular mechanisms. To that end, we tested whether the role of divalent ions in the strong intermonomer interaction originates from an electrostatic effect or involves coordination chemistry, possibly with the histidine residues that are abundant in the D4 domain (Fig. 1 *A*). We performed force experiments on A1-CK dimers at pH 7.4 in buffer solution supplemented with free Imidazole (200 mM) in addition to $MgCl_2$ and $CaCl_2$. In contrast to EDTA, which has only very low selectivity among the different divalent cations, Imidazole has virtually no affinity for Mg^{2+} and Ca^{2+} but is capable of forming strong coordination bonds with transition metal ions (37), which might be available during the biosynthesis of VWF. Strikingly, essentially only force-extension traces of type II were obtained (Figs. 5 *A* and S7), as inferred from a unimodal distribution of the position of the first A2 unfolding event (Fig. 5 *B*). Obstruction of the strong intermonomer interaction by free Imidazole was further corroborated by AFM imaging of full-length dimers adsorbed from the same buffer solution. In the presence of Imidazole, nearly all dimers exhibited a flexible conformation (Fig. 5, *C* and *D*), which is in line with a scenario in which divalent (transition) metals are involved in the formation of the strong intermonomer interaction.

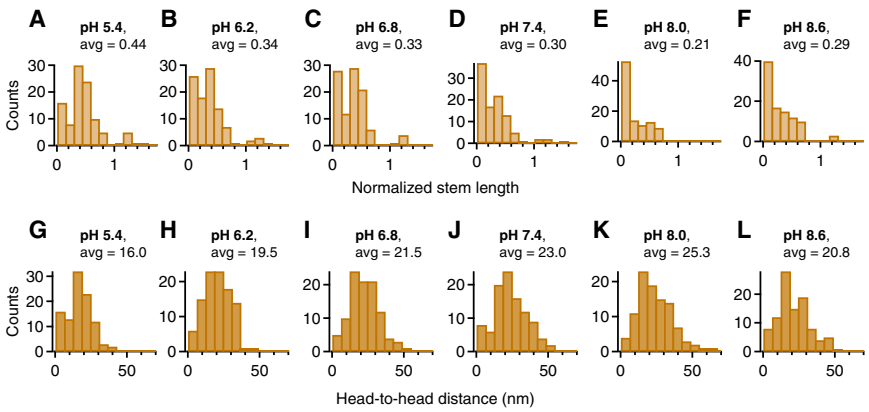

FIGURE 4 Impact of the pH on C-terminal stem formation within dimeric VWF constructs with a deletion of the D4 domain. (*A–F*) Distributions of the normalized stem length of dimeric delD4 constructs and respective average values obtained at pH 5.4 (*A*), 6.2 (*B*), 6.8 (*C*), 7.4 (*D*), 8.0 (*E*), and 8.6 (*F*), by tracing dimers in AFM images individually along their contour. It should be noted that at the alkaline pH values of 8.0 and especially 8.6, a nonnegligible fraction of molecules had to be discarded from analysis due to apparent self-aggregation. (*G–L*) Distributions of the head-to-head distance of dimeric delD4 constructs obtained at pH 5.4 (*G*), 6.2 (*H*), 6.8 (*I*), 7.4 (*J*), 8.0 (*K*), and 8.6 (*L*). Values of the head-to-head distance indicate the direct distance between the two positions within a dimer at which the stem regions adjoin to higher N-terminal domains. Consequently, the distributions of the head-to-head distance provide a means for estimating the effective concentrations of N-terminal domains. It should be noted that immobilization of VWF dimers on the PLL-coated mica substrate might not proceed identically under varying pH conditions, as VWF's net charge changes with pH. The low-pH conditions near VWF's pI may allow dimers to equilibrate more effectively than they would at higher pH values (11), where the higher (negative) net charge of VWF molecules might lead to faster trapping on the surface. Consequently, the actual difference between average head-to-head distances for varying pH conditions might be slightly higher than observed. To see this figure in color, go online.

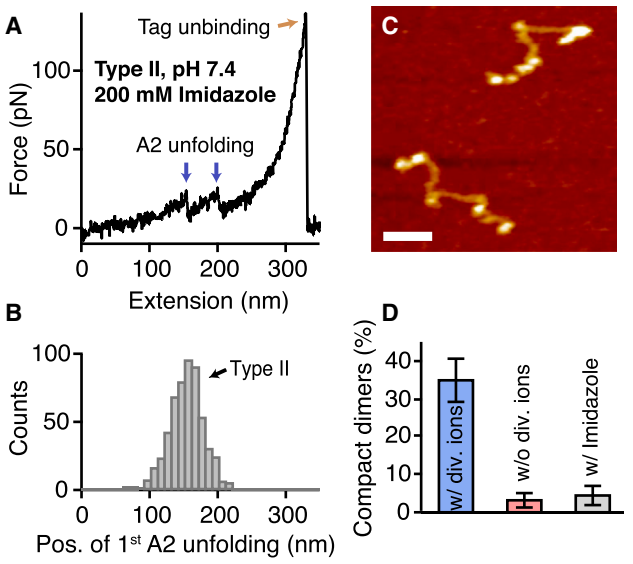

FIGURE 5 Obstruction of the strong intermonomer interaction by Imidazole. (*A* and *B*) Single-molecule force measurements on A1-CK dimers at pH 7.4 in the presence of divalent ions and 200 mM Imidazole. Force-extension traces of type II (*A*) were observed almost exclusively, as inferred from a unimodal distribution of the position of the first A2 unfolding peak (*B*). (*C* and *D*) AFM imaging of full-length VWF dimers adsorbed onto a functionalized mica surface from a buffer solution adjusted to pH 7.4 and containing 200 mM Imidazole in addition to divalent ions. Nearly all dimers exhibited a flexible conformation (*C*). Scale bar is 30 nm; range of color scale is 2.4 nm. The ratio of compact dimers was close to zero (*D*) ($n = 81$), which is similar to that obtained in the absence of divalent ions (see Fig. 3 *C*). Further coplotted is the markedly higher ratio observed for dimers adsorbed from buffer containing divalent ions but no Imidazole (see Fig. 3 *C*). Error bars represent Poisson noise (1 SD). To see this figure in color, go online.

DISCUSSION

In this work, we performed AFM-based single-molecule force measurements, AFM imaging, and SAXS to characterize VWF's force response and conformational ensemble under different pH conditions. We initially found that the mechanical resistance of VWF's dimeric subunits strongly depends on the pH, as quantified by the ratio of type I force-extension traces, i.e., traces corresponding to the force response of dimers that were initially firmly closed via the strong intermonomer interaction (13). Interestingly, at low pH values of 6.2 and 6.6, virtually no dimers exhibited the strong intermonomer interaction. At first glance, this finding may appear contradictory to the imaging data, which reveal that almost throughout the whole examined pH range, low pH favors a compact conformation of dimers, confirming a previous transmission electron microscopy study (7). In fact, combining the results from force and imaging experiments leads to the conclusion that compact dimers below pH 6.8 have a low mechanical resistance (Fig. 6, *top*) and, accordingly, that the strong intermonomer interaction in VWF dimers is absent at these low pH values. In other words, compactness of dimers under acidic pH conditions is not accomplished by the strong intermonomer interaction, suggesting that a second pH-dependent process promotes compactness under acidic pH conditions (7). Indeed, in the presence of divalent ions, the compactness of dimers as a function of the pH revealed two regimes, strongly suggesting that at least two pH-dependent interactions promote compactness.

The process that promotes compactness above pH 6.8 is the formation of the strong intermonomer interaction (Fig. 6, *bottom*), as inferred from two observations: first, the critical pH of 6.8, above which a second regime of compactness was observed, equals the critical pH of the strong intermonomer interaction observed in force experiments, and second, compactness above pH 6.8 can be abolished by taking out divalent ions from solution, in line with the loss of the strong intermonomer interaction observed in force experiments after treatment of samples with EDTA (13). In the absence of divalent ions, a monotonic decrease of the compactness of dimers with increasing pH was observed. The fact that this decrease was well described by the fit of a sigmoidal function suggests the existence of unidirectional, pH-dependent interactions that do not rely on divalent ions. AFM imaging experiments on dimeric delD4 constructs revealed a crucial role of the D4 domain in promoting compactness under acidic pH conditions. This finding strongly suggests the existence of a second intermonomer interaction mediated by D4 that is mechanically less stable than the strong intermonomer interaction.

Importantly, C-terminal stem formation by itself, based on weak interactions between C domains (13), was also affected by the pH, as revealed by distributions of the normalized stem length obtained for delD4 dimers under varying pH conditions. While at alkaline pH values the distributions exhibited an approximately exponential shape, decreasing the pH led to the emergence of a maximum corresponding to dimers possessing roughly half-formed stems, suggesting that the different C-domain interactions involved in stem formation are differently affected by the pH. Going along with this observation, the average value of the normalized stem length increased by trend with decreasing pH (Fig. 4), implying a decreased average distance between the two D4 domains within a full-length dimer. As a decreased distance between D4 domains in turn results in a higher effective concentration of these two putative binding partners, one could speculate that the pH dependence of the stem formation might be the only pH dependence underlying the increased compactness of dimers with decreasing pH. A simple estimation, based on the observed distances between N-terminal domains in a dimer (Fig. 4, *G–L*) and the assumption that the effective concentration of D4 scales with the inverse cube of these distances, suggests that the pH-induced changes of the distance between the D4 domains of a dimer may well lead to an increase of their effective concentration by a factor of 4 over the probed pH range. However, the strong pH dependence of the ratios of compact

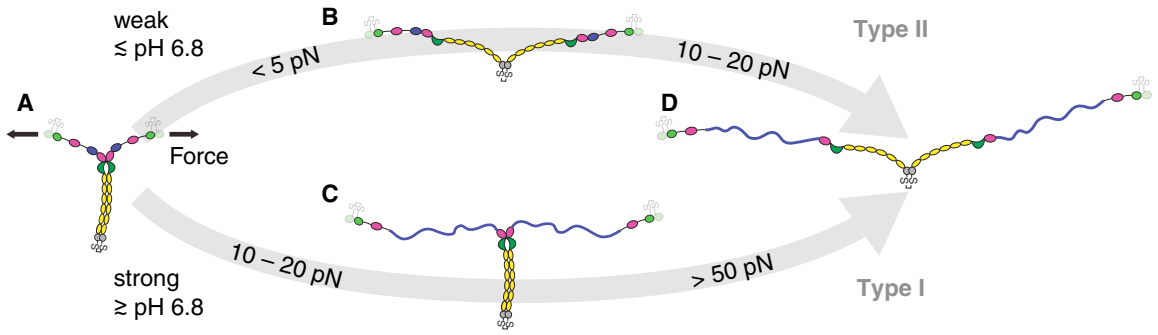

FIGURE 6 Strong and weak C-terminal rods in VWF's dimeric subunits. Schematically depicted are force-induced conformational changes (the indicated forces correspond to loading rates probed in single-molecule force experiments) of VWF dimers that initially possess a fully formed C-terminal stem (C-terminal rod) (*A*). At pH values below ~6.8, C-terminal rods are by trend weak and can dissociate at forces clearly below the detection limit of AFM force experiments, i.e., dissociation very likely occurs well below 5 pN (*B*). At forces of ~10–20 pN, VWF's A2 domains unfold and add a contour length of ~60–70 nm (lengths in the schematic are drawn roughly to scale) each to the elongation of dimers (14–17) (*D*). At pH values above ~6.8, however, C-terminal rods are by trend firmly closed via the strong intermonomer interaction. In this case, unfolding of the A2 domains at 10–20 pN is the first critical step of elongation (*C*). At forces above 50 pN, the strong intermonomer interaction can dissociate and add ~80 nm to the elongation of dimers (*D*). In the bloodstream, forces on VWF result from an interplay between elongational flow and length, implying a positive feedback between force and length. Therefore, for a VWF concatamer subjected to elongational flow under acidic pH conditions, forces of, e.g., 10–20 pN (as required for A2 unfolding), will be reached more readily than under near-physiological conditions, due to rapid initial opening of weak rods. To see this figure in color, go online.

dimers in the absence of divalent ions (Fig. 3 *C*, *red*) suggests that (assuming a constant affinity for the interaction between the two D4 domains) a change of the effective concentration by almost two orders of magnitude would be necessary to explain the observed increase of compactness with decreasing pH. Therefore, we assume that the mechanically weak intermonomer interaction mediated by D4 under acidic conditions possesses an intrinsic pH dependence. Remarkably, the direction of this pH dependence is the opposite of that of the strong intermonomer interaction mediated by the same domain. The pH dependence of both the weak D4-mediated interaction and stem formation may play a pivotal role in orderly multimerization and packing of VWF in the *trans*-Golgi and WPB (7).

Undoubtedly, a key finding of this study is the pH dependence of the strong intermonomer interaction in VWF's dimeric subunits. Strikingly, decreasing the pH from 7.4 by less than one unit switches off the strong intermonomer interaction, thereby drastically decreasing the mechanical resistance of dimers. While the strong intermonomer interaction was virtually not observed at pH 6.6, it could form again after a buffer exchange to buffer solution adjusted to pH 7.4. This finding indicates that the molecular mechanisms that underlie the pH dependence of the strong intermonomer interaction are largely reversible. Importantly, the key domain D4 possesses a high density of histidine residues whose Imidazole side chains can be protonated, resulting in a change of their net charge, at a pH of ~6.5 (the pK_a value of free histidines (38)). This value is very close to the pH range over which the strong intermonomer interaction was abruptly switched off. A possible role of histidines was indeed indicated by measurements in the presence of free Imidazole, which revealed obstruction of the strong intermonomer interaction. Given that the strong intermonomer interaction crucially depends on divalent ions (13), we propose that the coordination of metal ions by histidine residues may play a fundamental role in the formation of the strong intermonomer interaction. Indeed, it is well-known that coordination chemistry through Imidazole is impeded by protonation. It should be noted that full obstruction of the strong intermonomer interaction by removal of divalent ions was not achieved by a simple buffer exchange to buffer that did not contain divalent ions, and instead required the addition of EDTA (see Materials and Methods, "Buffers"). This implies that ion species that were not added to our buffer solutions (e.g., ions of transition metals such as zinc) could also be involved in the formation of the strong intermonomer interaction. We further note that one should take the effect of Imidazole into account when using it in protein purification procedures.

Histidine residues might also play a role in mediating the increase in compactness of dimers under acidic conditions, as suggested by the sigmoidal fit to the data obtained in the absence of divalent ions, which reached its half-maximum value at a pH of ~6.6, close to the pK_a value of histidines. We believe that high-resolution structures, especially of the D4 domain and its constituent modules, will be of great value for elucidating the pH dependencies within VWF.

In the vasculature, activation of VWF for hemostasis crucially depends on its ability to sense hydrodynamic forces (1,2,39) originating from an interplay of concatamer length and elongational flow components (14,40,41). Importantly, force sensing by VWF is tuned by the strong intermonomer interaction in its dimeric subunits, as it markedly shortens the effective length of a concatamer contributing to force sensing (13). For the pH values probed in our experiments, the fraction of firmly closed dimers reached a maximum at a pH of 7.4, indicating that VWF's mechanical

resistance is maximized with respect to the physiological pH of 7.4 in the blood. Accordingly, the critical rates of elongational flow needed to activate VWF for hemostasis, i.e., to initiate collagen binding and platelet aggregation, will be highest at physiological pH, assuming that the interactions of VWF with collagen and platelets as such remain unvaried by the pH.

It is tempting to speculate about the role of this pH dependence, considering that the pH may be disturbed locally at sites of vascular injury. Indeed, it is widely accepted that local pH variations, especially acidification, occur in connection with injury and inflammation (20–24), although it remains unclear to what extent and on which timescales the blood pH may be affected. Our data suggest that deviations from physiological pH will lower the critical rates of elongational flow to activate VWF for hemostasis. In particular, acidification is expected to reduce such critical elongational flow rates very effectively. Indeed, data obtained from flow experiments and published within the framework of a PhD thesis (42) suggest that critical shear rates for elongation of VWF are lowered upon both acidification and alkalization. In principle, the relative impact of the pH on critical elongational flow rates can be estimated based on the ratio of firmly closed dimers in VWF observed at a given pH (13). For instance, at a pH of 6.6, where virtually no dimers exhibit the strong intermonomer interaction, the critical elongational flow may only be roughly half that observed at pH 7.4, as in the latter case VWF's effective force-sensing length is expected to be decreased by ~30%, assuming that approximately half of VWF's dimeric subunits are firmly closed via the strong intermonomer interaction. It should be noted that under acidic conditions, VWF's force-sensing length will initially be lower than under physiological conditions, due to compact yet mechanically relatively unstable dimers. However, as strongly suggested by our force data, most compact dimers below pH 6.8 will open up at comparably very low elongational flow rates and consequently increase VWF's effective force-sensing length very rapidly, thereby triggering further elongation, due to the positive feedback between hydrodynamic force and length. In a nutshell, one could speculate that VWF's pH-dependent elongation behavior represents a smart means to enhance VWF's hemostatic activity where needed.

In summary, the structure and mechanics of VWF are governed primarily by two distinct intermonomer interactions within its dimeric subunits (Fig. 6). Remarkably, the two interactions exhibit opposite pH dependencies while at the same time they both appear to be mediated by modules of VWF's D4 domain. Strikingly, decreasing the pH by one unit from physiological pH yields a markedly increased degree of compactness of dimers but a considerably decreased mechanical stability. While high compactness at acidic pH can be assumed to be a prerequisite for orderly multimerization in the *trans*-Golgi and storage in Weibel-Palade bodies, low mechanical resistance at acidic pH may enhance VWF's hemostatic activity at sites of locally lowered pH encountered in the wake of injuries. Therefore, our data should provide further insights into VWF's activation for hemostasis.

SUPPORTING MATERIAL

Seven figures are available at http://www.biophysj.org/biophysj/supplemental/S0006-3495(16)30468-4.

AUTHOR CONTRIBUTIONS

J.P.M. and A.L. designed experiments; acquired, analyzed, and interpreted AFM force and imaging data; and wrote the manuscript with input from coauthors. S.M. acquired and analyzed force data. T.O. designed and prepared constructs. L.K.B. acquired and analyzed SAXS data. W.V. designed imaging experiments and interpreted data. J.L. designed SAXS experiments and analyzed data. R.S. and M.B. designed the overall research.

ACKNOWLEDGMENTS

We are very grateful to Prof. Dr. Hermann E. Gaub and Prof. Dr. Erich Sackmann for helpful discussions. We thank Prof. Dr. Matthias F. Schneider and Dr. Volker Huck for fruitful conversations. Gesa König is acknowledged for technical assistance in preparing recombinant VWF. We thank Dr. Diana A. Pippig for providing tetravalent Strep-Tactin with a single cysteine, Thomas Nicolaus for technical assistance in protein purification, and Lukas Milles for sharing a data-processing and denoising algorithm. We also thank Dr. Cy M. Jeffries and Dr. Marianne Liebi for support at SAXS beamlines P12 and X12SA, respectively.

This study was supported by research funding from the German Research Foundation to the Research Group FOR1543 ("Shear Flow Regulation of Hemostasis—Bridging the Gap between Nanomechanics and Clinical Presentation") and to the Nanosystems Initiative Munich (NIM). Support was also provided by the Center for Nanoscience (CeNS). W.V. received a postdoctoral fellowship and a travel grant from the Research Foundation Flanders.

REFERENCES

1. Springer, T. A. 2014. von Willebrand factor, Jedi knight of the bloodstream. *Blood.* 124:1412–1425.
2. Schneider, S. W., S. Nuschele, …, M. F. Schneider. 2007. Shear-induced unfolding triggers adhesion of von Willebrand factor fibers. *Proc. Natl. Acad. Sci. USA.* 104:7899–7903.
3. Ruggeri, Z. M., J. N. Orje, …, A. J. Reininger. 2006. Activation-independent platelet adhesion and aggregation under elevated shear stress. *Blood.* 108:1903–1910.
4. Sadler, J. E. 1998. Biochemistry and genetics of von Willebrand factor. *Annu. Rev. Biochem.* 67:395–424.
5. Wagner, D. D. 1990. Cell biology of von Willebrand factor. *Annu. Rev. Cell Biol.* 6:217–246.
6. Huang, R.-H., Y. Wang, …, J. E. Sadler. 2008. Assembly of Weibel-Palade body-like tubules from N-terminal domains of von Willebrand factor. *Proc. Natl. Acad. Sci. USA.* 105:482–487.
7. Zhou, Y.-F., E. T. Eng, …, T. A. Springer. 2011. A pH-regulated dimeric bouquet in the structure of von Willebrand factor. *EMBO J.* 30:4098–4111.
8. Lippok, S., K. Kolšek, …, M. A. Brehm. 2016. von Willebrand factor is dimerized by protein disulfide isomerase. *Blood.* 127:1183–1191.

9. Springer, T. A. 2011. Biology and physics of von Willebrand factor concatamers. *J. Thromb. Haemost.* 9 (*Suppl 1*):130–143.
10. Erent, M., A. Meli, …, T. Carter. 2007. Rate, extent and concentration dependence of histamine-evoked Weibel-Palade body exocytosis determined from individual fusion events in human endothelial cells. *J. Physiol.* 583:195–212.
11. Fulcher, C. A., Z. M. Ruggeri, and T. S. Zimmerman. 1983. Isoelectric focusing of human von Willebrand factor in urea-agarose gels. *Blood.* 61:304–310.
12. Zhou, Y.-F., E. T. Eng, …, T. A. Springer. 2012. Sequence and structure relationships within von Willebrand factor. *Blood.* 120:449–458.
13. Müller, J. P., S. Mielke, …, M. Benoit. 2016. Force sensing by the vascular protein von Willebrand factor is tuned by a strong intermonomer interaction. *Proc. Natl. Acad. Sci. USA.* 113:1208–1213.
14. Zhang, X., K. Halvorsen, …, T. A. Springer. 2009. Mechanoenzymatic cleavage of the ultralarge vascular protein von Willebrand factor. *Science.* 324:1330–1334.
15. Ying, J., Y. Ling, …, J.-Y. Shao. 2010. Unfolding the A2 domain of von Willebrand factor with the optical trap. *Biophys. J.* 98:1685–1693.
16. Jakobi, A. J., A. Mashaghi, …, E. G. Huizinga. 2011. Calcium modulates force sensing by the von Willebrand factor A2 domain. *Nat. Commun.* 2:385.
17. Xu, A. J., and T. A. Springer. 2012. Calcium stabilizes the von Willebrand factor A2 domain by promoting refolding. *Proc. Natl. Acad. Sci. USA.* 109:3742–3747.
18. Sing, C. E., and A. Alexander-Katz. 2010. Elongational flow induces the unfolding of von Willebrand factor at physiological flow rates. *Biophys. J.* 98:L35–L37.
19. Huck, V., M. F. Schneider, …, S. W. Schneider. 2014. The various states of von Willebrand factor and their function in physiology and pathophysiology. *Thromb. Haemost.* 111:598–609.
20. Christou, H., N. Bailey, …, S. Kourembanas. 2005. Extracellular acidosis induces heme oxygenase-1 expression in vascular smooth muscle cells. *Am. J. Physiol. Heart Circ. Physiol.* 288:H2647–H2652.
21. Babich, V., L. Knipe, …, T. Carter. 2009. Differential effect of extracellular acidosis on the release and dispersal of soluble and membrane proteins secreted from the Weibel-Palade body. *J. Biol. Chem.* 284:12459–12468.
22. Serrano, C. V., Jr., A. Fraticelli, …, M. C. Capogrossi. 1996. pH dependence of neutrophil-endothelial cell adhesion and adhesion molecule expression. *Am. J. Physiol.* 271:C962–C970.
23. Ihrcke, N. S., W. Parker, …, J. L. Platt. 1998. Regulation of platelet heparanase during inflammation: role of pH and proteinases. *J. Cell. Physiol.* 175:255–267.
24. De Backer, D. 2003. Lactic acidosis. *Minerva Anestesiol.* 69:281–284.
25. Baumann, F., M. S. Bauer, …, D. A. Pippig. 2016. Monovalent Strep-Tactin for strong and site-specific tethering in nanospectroscopy. *Nat. Nanotechnol.* 11:89–94.
26. Zimmermann, J. L., T. Nicolaus, …, K. Blank. 2010. Thiol-based, site-specific and covalent immobilization of biomolecules for single-molecule experiments. *Nat. Protoc.* 5:975–985.
27. Gumpp, H., S. W. Stahl, …, H. E. Gaub. 2009. Ultrastable combined atomic force and total internal reflection fluorescence microscope [corrected]. *Rev. Sci. Instrum.* 80:063704.
28. Hutter, J. L., and J. Bechhoefer. 1993. Calibration of atomic-force microscope tips. *Rev. Sci. Instrum.* 64:1868–1873.
29. Condat, L. 2013. A direct algorithm for 1D total variation denoising. *IEEE Signal Process. Lett.* 20:1054–1057.
30. Blanchet, C. E., A. Spilotros, …, D. I. Svergun. 2015. Versatile sample environments and automation for biological solution X-ray scattering experiments at the P12 beamline (PETRA III, DESY). *J. Appl. Cryst.* 48:431–443.
31. Konarev, P. V., V. V. Volkov, …, D. I. Svergun. 2003. PRIMUS: a Windows PC-based system for small-angle scattering data analysis. *J. Appl. Cryst.* 36:1277–1282.
32. Yin, J., P. D. Straight, …, C. T. Walsh. 2005. Genetically encoded short peptide tag for versatile protein labeling by Sfp phosphopantetheinyl transferase. *Proc. Natl. Acad. Sci. USA.* 102:15815–15820.
33. Schmidt, T. G. M., L. Batz, …, K. Stanar. 2013. Development of the Twin-Strep-tag® and its application for purification of recombinant proteins from cell culture supernatants. *Protein Expr. Purif.* 92:54–61.
34. Kim, M., C. C. Wang, …, P. E. Marszalek. 2012. A nanoscale force probe for gauging intermolecular interactions. *Angew. Chem. Int. Ed. Engl.* 51:1903–1906.
35. Lipfert, J., and S. Doniach. 2007. Small-angle X-ray scattering from RNA, proteins, and protein complexes. *Annu. Rev. Biophys. Biomol. Struct.* 36:307–327.
36. Mertens, H. D. T., and D. I. Svergun. 2010. Structural characterization of proteins and complexes using small-angle X-ray solution scattering. *J. Struct. Biol.* 172:128–141.
37. Schmitt, L., M. Ludwig, …, R. Tampé. 2000. A metal-chelating microscopy tip as a new toolbox for single-molecule experiments by atomic force microscopy. *Biophys. J.* 78:3275–3285.
38. Srivastava, J., D. L. Barber, and M. P. Jacobson. 2007. Intracellular pH sensors: design principles and functional significance. *Physiology (Bethesda).* 22:30–39.
39. Ruggeri, Z. M. 1997. von Willebrand factor. *J. Clin. Invest.* 99:559–564.
40. Perkins, T. T., D. E. Smith, and S. Chu. 1997. Single polymer dynamics in an elongational flow. *Science.* 276:2016–2021.
41. Smith, D. E., H. P. Babcock, and S. Chu. 1999. Single-polymer dynamics in steady shear flow. *Science.* 283:1724–1727.
42. Steppich, D. M. 2009. The Physics of Von Willebrand Factor (VWF). PhD thesis, University of Augsburg, Augsburg, Germany.